CrystEngComm

RSC Publishing

PAPER

Coordination polymers based on 3,3′,4,4′-benzophenone-tetracarboxylate and N-containing pillars: syntheses, structure, characterization and properties†

Cite this: *CrystEngComm*, 2013, **15**, 7505

Li-Rong Yang,* Huai-Min Zhang, Qian-qian You, Lan-Zhi Wu, Liu Liu and Shuang Song

Received 14th March 2013,
Accepted 18th July 2013

DOI: 10.1039/c3ce40456k

www.rsc.org/crystengcomm

Three novel coordination polymers including $\{[Mn_2(bptc)_2(phen)_4]\cdot 2H_2O\}_\infty$ (**I**), $[Zn_2(bptc)_4\cdot(bpy)_2\cdot H_2O]_\infty$ (**II**), and $\{[Zn_2(bptc)_4\cdot(bpy)_2\cdot H_2O] \supset bpy\}_\infty$ (**III**) (bptc = 3,3′,4,4′-benzophenone-tetracarboxylate, bpy = 4,4′-bipyridine, phen = 1,10-phenanthroline) were prepared under hydrothermal conditions and characterized by elemental analysis, infrared spectrometry, and single crystal X-ray diffraction. Moreover, the thermal stability of as-synthesized coordination polymers was evaluated by thermogravimetric analysis; and their magnetic and luminescent properties were also investigated. Findings indicate that coordination polymer **I** displays a three-dimensional (3D) network constructed *via* π–π interactions of the building block $\{[Mn_2(bptc)_2(phen)_4]\cdot 2H_2O\}$. Besides, Zn(1) and Zn(2) centers in coordination polymer **II** are four-coordinated and six-coordinated, respectively, thereby affording two-dimensional (2D) planar sheet and 3D porous frameworks that are interlinked through identical linkers of four-coordinated motif (COO–Zn–COO). As-synthesized coordination polymer **III** contains a 3D framework similar to that of **II**, but the cavities in **III** are occupied by uncoordinated bpy guest molecules. Moreover, as-synthesized coordination polymer **I** presents antiferromagnetic coupling through the $(O_2C–C–C–CO_2)_2$ bridges, and **II** displays selectivity towards Hg^+ ion in terms of the luminescent emission.

Introduction

The crystal engineering of porous coordination polymers is becoming an increasingly popular field of research in recent years, due to their intriguing aesthetic and potential applications in diverse areas such as catalysis, optoelectronics, supramolecular storage of molecules, molecular magnetism, gas storage, chemical separations, ion exchange, microelectronics, nonlinear optics and heterogeneous catalysis.[1–7]

The construction of coordination polymers is highly influenced by many factors such as the coordination nature of metal ions, the structural characteristics of multidentate organic ligands, metal–ligand ratio and counterions.[6,8–13] Usually, multidentate organic ligands like polybasic carboxylic acids are recommended as the linkers for metal ions to polymerize into extended open frameworks, because these ligands may potentially provide various coordination modes and favor the construction of multi-dimensional coordination polymers.[7,14–26] In this respect, H_4bptc (bptc = 3,3′,4,4′-benzophenone-tetracarboxylate) is particularly significant. This is because, firstly, H_4bptc can be partially or completely deprotonated to generate H_3bptc^-, H_2bptc^{2-}, $Hbptc^{3-}$ and $bptc^{4-}$ when the pH value is carefully controlled, which provides H_4bptc with various acidity-dependant coordination modes; not to mention that H_4bptc in the synthetic system acts not only as a necessary coordination ligand but also as a pH value adjuster of the reaction mixture.[8] Secondly, the two benzene rings connected to the four carboxylic groups and the steric effect between the two adjacent carboxylic groups of H_4bptc, an asymmetrically V-shaped ligand, may allow bptc to link metal ions in different directions, thereby inducing a dissymmetric unit for metal atoms to improve the helicity of polymeric chains and favor the formation of a helical structure. Thirdly, the flexible multidentate coordination sites of H_4bptc can provide a high possibility for multi-dimensional networks to form. In addition, few are currently available about the coordination chemistry of H_4bptc, which means it is imperative to acquire more insights into H_4bptc as a desired ligand to construct multi-dimensional coordination polymers.[12,15,16,18,27–36] In the meantime, the introduction of

Henan Key Laboratory of Polyoxometalate, Institute of Molecule and Crystal Engineering, College of Chemistry and Chemical Engineering, Henan University, Kaifeng 475004, P. R. China. E-mail: lirongyang@henu.edu.cn

† Electronic supplementary information (ESI) available. CCDC 857478, 863678 and 871939 contain the supplementary crystallographic data for this paper. For ESI and crystallographic data in CIF or other electronic format see DOI: 10.1039/c3ce40456k

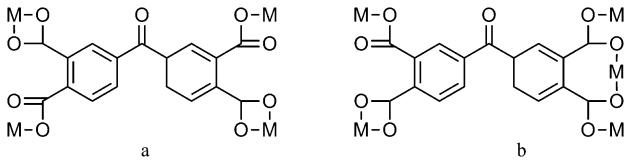

Scheme 1 Coordination modes of bptc ligand in coordination polymers **I–III**.

N-containing auxiliary ligands (for example, 4,4′-bipyridine and 1,10-phenanthroline) into the reaction system may result in many novel frameworks, thanks to many superiorities of N-containing auxiliary ligands.[10,13,37–40]. On the one hand, N-containing auxiliary ligands as rigid rodlike bifunctional ligands can be well employed to construct one-dimensional (1D) linear polymeric chains thereby facilitating assembly of coordination polymers. On the other hand, N-containing auxiliary ligands contain oriented pyridine rings that provide feasibility for lower dimensional networks to be extended into multi-dimensional ones. Furthermore, pyridine rings are superior in terms of hydrogen-bonding formation and π–π stacking interactions that are significant for affording extended open frameworks *via* polymerization.[41–43]

Therefore, we are particularly interested in constructing thermodynamically stable nanoporous coordination polymers based on H_4bptc multidentate organic ligand and N-containing auxiliary ligands. This article reports the hydrothermal synthesis and characterization of 3D coordination polymers of Mn(II) and Zn(II) centers with H_4bptc, 4,4′-bipyridine and 1,10-phenanthroline ligands under different temperatures. Besides, it also reports the thermal stability, magnetic property and luminescent properties of as-synthesized coordination polymers involving $\{[Mn_2(bptc)_2(phen)_4]\cdot 2H_2O\}_\infty$ (**I**), $[Zn_2(bptc)_4\cdot(bpy)_2\cdot H_2O]_\infty$ (**II**), and $\{[Zn_2(bptc)_4\cdot(bpy)_2\cdot H_2O] \supset bpy\}_\infty$ (**III**). The typical coordination modes of H_4bptc in the coordination polymers (mode a and mode b) are summarized in Scheme 1.

Results and discussion

Infrared (IR) spectra of as-synthesized coordination polymers

Coordination polymers **I**, **II**, and **III** are stable in the solid state upon exposure to air and are insoluble in common organic solvents such as CH_3COCH_3, CH_3CH_2OH, CH_3OH, CH_3CN, tetrahydrofuran, dimethyl sulfoxide and dimethylformamide. IR spectra of solid state **I–III** recorded in the range of 4000–400 cm^{-1} suggest that there exists $bptc^{4-}$ in as-synthesized coordination polymers **I–III**. Besides, phen (phen = 1,10-phenanthroline) ligand of **I** and bpy (bpy = 4,4′-bipyridine) ligand of **II** and **III** are coordinated to central Mn(II) or Zn(II) ions,[44–53] respectively, which is also evidenced by relevant X-ray diffraction measurements.[54]

Structural description of coordination polymers I, II and III

$\{[Mn_2(bptc)_2(phen)_4]\cdot 2H_2O\}_\infty$ (I). Single-crystal X-ray structural analysis shows that the asymmetrical unit in **I** contains two seven-coordinated Mn(II) ions. The Mn(II) center adopts a slightly distorted N_4O_3 pentagonal bipyramidal geometry, and the bptc ligand adopts μ_4-$bptc^{4-}$ coordination mode (see Scheme 1a and Fig. S1, ESI†). The axial positions are occupied by N(1) and O(4) atoms (from phen and μ_4-$bptc^{4-}$, respectively), while the equatorial plane consists of N(2), N(3) and N(4) (from two phen ligands) and O(2), O(3) (from μ_4-$bptc^{4-}$ ligand). Mn–N bond lengths fall in the range of 2.294–2.468 Å, and Mn–O bond lengths are in the range of 2.105–2.791 Å (see Table 2), which is in accordance with what is reported elsewhere.[55,56] In the unit of $[Mn_2(bptc)_2(phen)_4]$, there exists

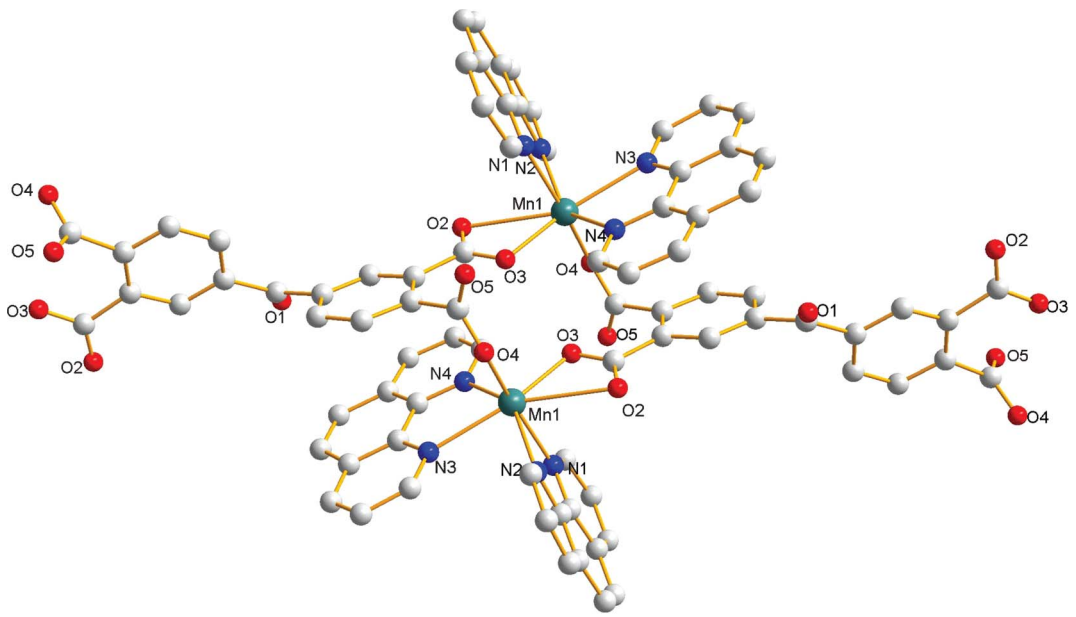

Fig. 1 Diagram showing the coordination environments for Mn(II) centers in **I**. All hydrogen atoms and lattice-water molecules are omitted for clarity.

a closed 14-numbered ring with an approximate dimension of 5.230(9) × 7.007(4) Å^2 between two Mn(II) centers (ring (COO)$_2$–Mn–(COO)$_2$–Mn, as illustrated in Fig. 1), and this ring contains two molecules of μ_4-bptc^{4-} ligand. Based on the building block of {[Mn$_2$(bptc)$_2$(phen)$_4$]·2H$_2$O}, **I** is connected by four COO$^-$ groups from two molecules of μ_4-bptc^{4-} to generate a one-dimensional (1D) infinite ribbon (Fig. 2b), *i.e.*, {[Mn$_2$(bptc)$_2$(phen)$_4$]·2H$_2$O}$_\infty$. The 1D units are further linked into two-dimensional (2D) sheets through the linkers of 8-numbered hydrogen bonding ring formed by two lattice water molecules and two COO$^-$ groups (see Fig. 2a and 2c). The adjacent 2D sheets are interconnected into three-dimensional (3D) networks through π–π interactions between parallel pyridine rings in phen with the face-to-face distances of 3.757 Å (Fig. S3, ESI†). Besides, self-penetrating occurs in the topological graph of 3D networks, as shown in Fig. 2d and Table 3 **I–III**.

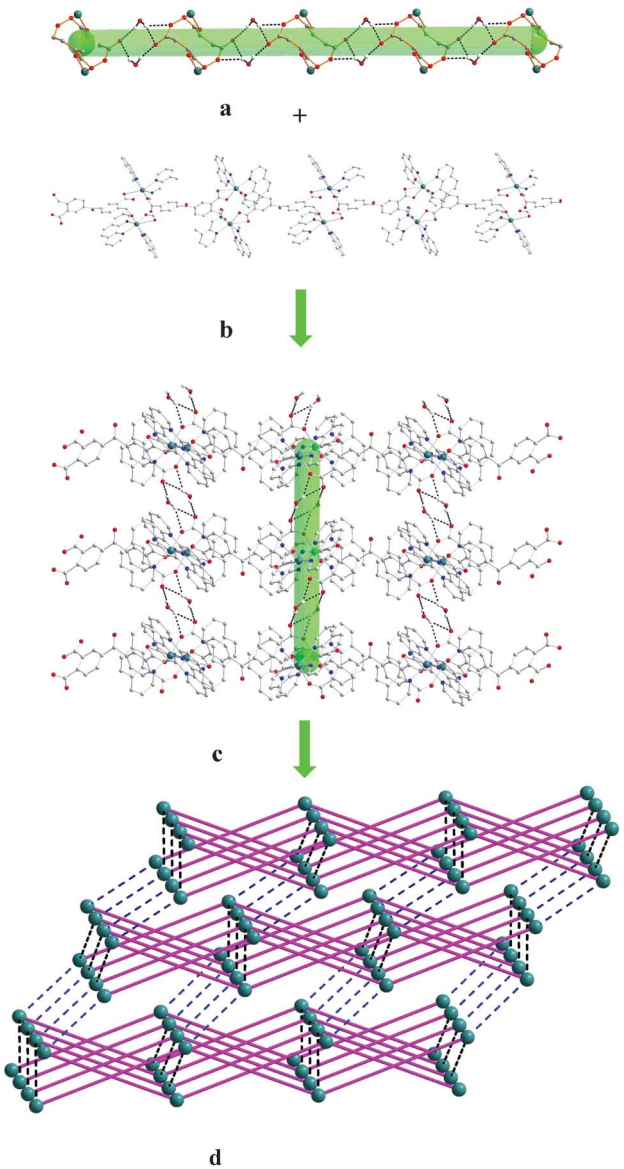

Fig. 2 (a) 8-Numbered hydrogen bonding ring; (b) view of 1D infinite chain of {[Mn$_2$(bptc)$_2$(phen)$_4$]·2H$_2$O}$_\infty$ in **I**; (c) diagram showing the 2D sheet connected through 8-numbered hydrogen bonding rings between the adjacent chains; (d) topological graph of **I** showing the 3D architecture. All hydrogen atoms and lattice-water molecules are omitted for clarity.

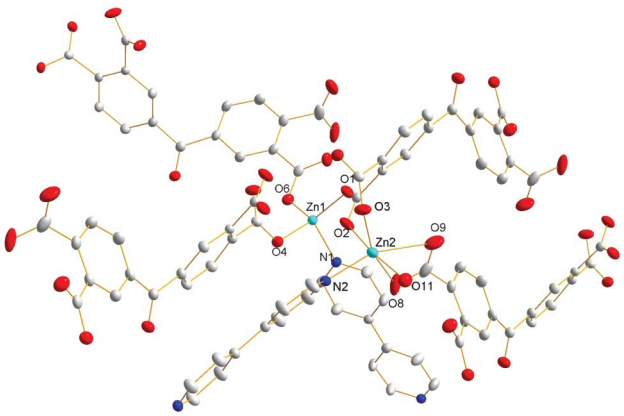

Fig. 3 Diagram showing the coordination environments of Zn(II) centers in **II**. All hydrogen atoms are omitted for clarity.

[Zn$_2$(bptc)$_4$·(bpy)$_2$·H$_2$O]$_\infty$ (II). Single-crystal analysis reveals that coordination polymer **II** exhibits a 3D self-penetrating network, and its Zn(II) centers adopt significantly different coordination environments (Fig. 3 and S2, ESI†). Namely, there are two unique Zn(II) ions in the asymmetric unit: Zn(1) is four-coordinated with the N$_1$O$_3$ donor set to feature a distorted tetrahedral geometry, and Zn(2) is six-coordinated with the N$_1$O$_5$ donor set to give rise to a distorted octahedral configuration. Besides, all the V-shaped μ_5-bptc^{4-} ligands adopt identical coordination modes around both Zn(II) ions (mode b), as shown in Scheme 1. The two Zn(II) ions are well-separated, and the nonbonding distance of Zn(1)···Zn(2) is 4.978(7) Å. The bond lengths of Zn(1)–O and Zn(1)–N are 1.956(2)–1.982(2) Å and 2.040(2) Å; and those of Zn(2)–O and Zn(2)–N are 1.989(2)–2.487(3) Å and 2.053(2) Å. Obviously, Zn(2) has much larger bond lengths than Zn(1), which is mainly because they possess different coordination environments and geometries. Moreover, the bond length data in the present research is consistent with those in previous research about coordination polymers containing Zn(II) ions.[20,57,58]

In terms of the framework of coordination polymer **II**, Zn(1) and Zn(2) are connected through carboxylic oxygen bridges (O(1)–C(1)–O(2) in μ_2-(η^1-O),(η^1-O′) fashion) from one μ_5-bptc^{4-} ligand to propagate an infinite 1D looped ribbon whose two types of rings are alternately arranged in the pattern of (ABAB)$_\infty$. Namely, 32-numbered ring A consists of Zn$_2$–(CO$_2$–C–C–CO$_2$)$_2$–(μ_2-bpy)$_2$ and 28-numbered ring B consists of Zn$_2$–(μ_5-bptc^{4-})$_2$, and their dimensions are approximately 16.329(4) × 7.337(4) Å^2 and 12.0056(1) × 6.4271(4) Å^2, respectively (see Fig. 4a). Furthermore, the motif of COO–Zn–COO (Zn(II) ion adopting 4-coordinated fashion) acts as the linker to concatenate the adjacent ribbons into 2D planar sheets which are further interlinked up and down into a 3D porous framework (see Fig. 4b and 4c).

It is noteworthy that the dihedral angle between two phenyl rings of the same μ_4-bptc^{4-} unit twists by 64.462(9)° from each

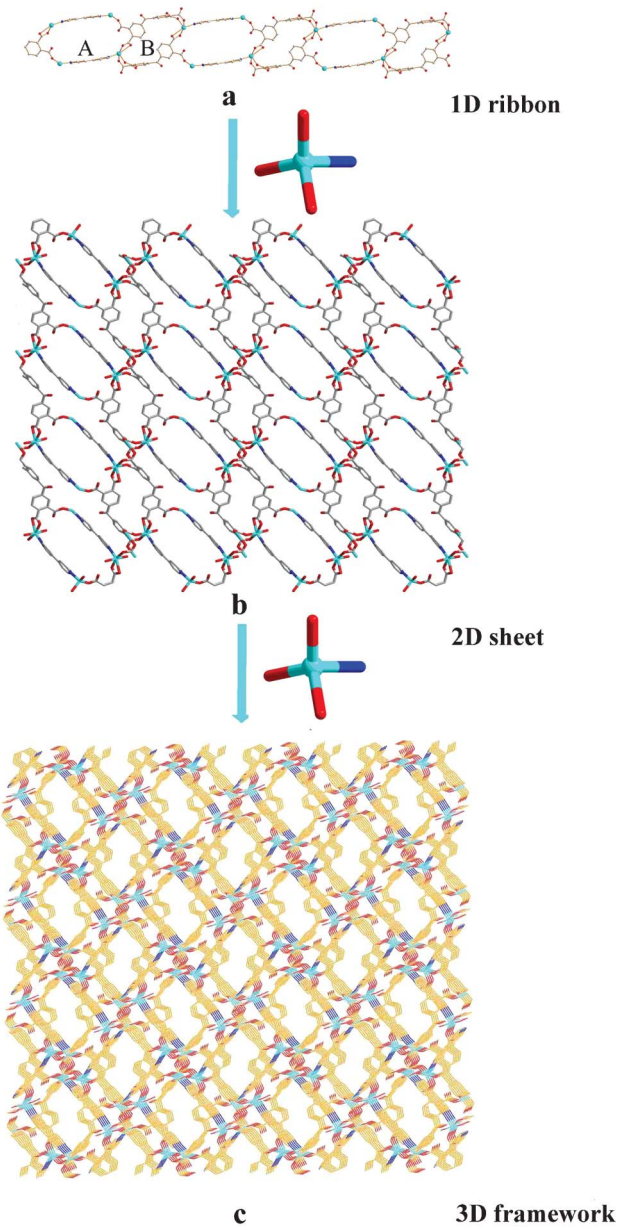

Fig. 4 (a) View of 1D infinite ribbon comprising of two types of rings in **II**; (b) diagram showing the 2D sheet connected through COO–Zn–COO linkers between adjacent ribbons; and (c) 3D porous framework generated based on COO–Zn–COO linkers. All hydrogen atoms are omitted for clarity.

other. The torsion angles between COO^- groups and phenyl ring range from 18.193(2)° to 64.327(2)°, and the angles between adjacent COO^- groups are 70.196(3)° and 77.039(3)°, respectively. Besides, the severely twisted V-shaped μ_4-bptc^{4-} unit results in wavelike 2D layer network; and all μ_5-bptc^{4-} ligands generate wavy lines while all 6-coordinated Zn(II) moieties are located therein (see Fig. 5). Furthermore, the pink wavy chains are reciprocally parallel, and the distance between two adjacent pink wave chains is 15.026(2) Å. Similarly, the green wavy chains are also reciprocally parallel, and the distance between two adjacent green wave chains is also 15.026(2) Å. Moreover, the two types of adjacent wavy chains

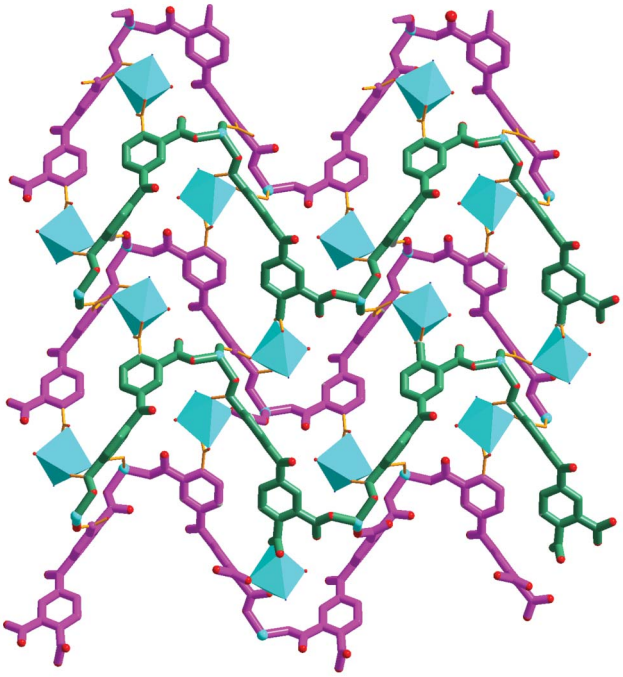

Fig. 5 View of 2D wavelike sheet generated from wavy chains by way of COO–Zn–COO linkers.

are further pillared alternately into a malposed double-layered motif by way of 4-coordinated COO–Zn–COO linkers.

{[Zn_2(bptc)$_4$·(bpy)$_2$·H_2O] ⊃ bpy}$_\infty$ (III). Coordination polymer **III** is synthesized under experimental procedures similar to those of **II** except that different molar ratio of zinc acetate to bpy ligand is adopted (molar ratio of zinc acetate to bpy is 1 : 1 for **II** and 1 : 2 for **III**). As a result, Zn(II) ions in **II** and **III** have similar coordination environments (Zn(1) is four-coordinated with a distorted tetrahedral geometry, while Zn(2) is six-coordinated with a distorted octahedral configuration), and the coordination modes of μ_4-bptc^{4-} unit as well as the framework structure of 1D ribbon, 2D sheet and 3D networks are also similar in **II** and **III** (see Fig. 6a–6d). Nevertheless, there still exist some significant differences in terms of the coordination chemistry of **II** and **III**. Similar to what is mentioned above for coordination polymer **II**, the 4-coordinated COO–Zn–COO linker in **III** also integrates 1D ribbons into 2D sheets and ultimately into a 3D architecture thereby constructing nanosized cavities (the 32-numbered ring) with an approximate dimension of 16.264(4) × 7.079(3) Å^2 and allowing accommodation of uncoordinated bpy guest molecules. However, bpy ligand in **III** acts not only as μ_2-bridging ligand to support the framework but also as guest molecule to effectively fill the nanosized cavities (similar cavities in **II** are guest-free). Besides, the coordinated μ_2-bridging bpy molecules in **III** are connected with the guest bpy molecules through π–π interactions, and the face-to-face distance between their parallel pyridine rings is 3.556 Å (as illustrated in Fig. 6b and 6c). Such a difference between the cavities of **III** and **II** is mainly attributed to the ratio-dependent and guest-driven synergistic effects during the assembly process of the

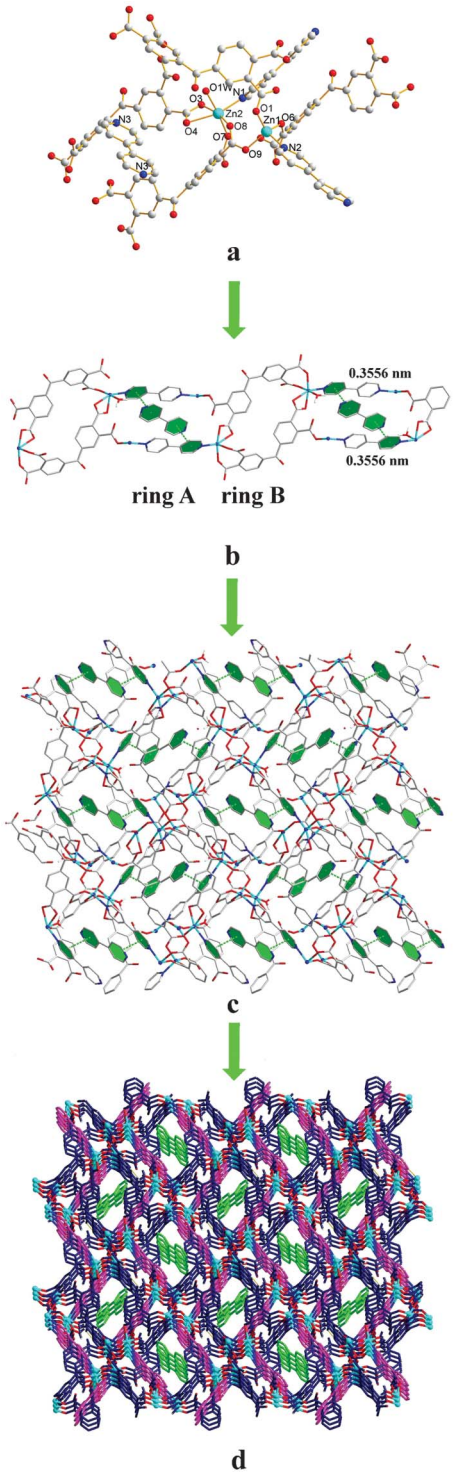

Fig. 6 (a) Diagram showing the coordination environments of Zn(II) centers in **III**; (b) π–π interactions between coordinated bpy molecules and guest-bpy molecules; (c) diagram showing the 2D sheet connected *via* COO–Zn–COO linkers between the adjacent chains; (d) perspective view of the 3D network in **III** (the 1D cavities occupied by the uncoordinated guest-bpy molecules are highlighted). All hydrogen atoms are omitted for clarity.

coordination polymers.[59] Moreover, the Zn–O bond in **III** (2.060 Å) is shorter than that in **II** (2.087 Å), and the Zn–N bond in **III** (2.047 Å) is slightly longer than that in **II** (2.044 Å),

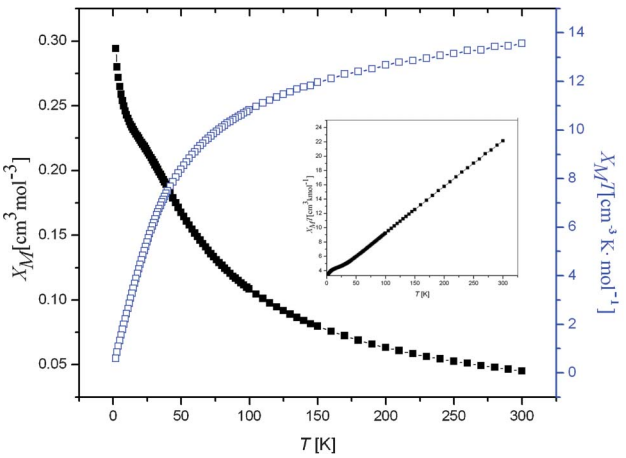

Fig. 7 Thermal variation of χ_M and $\chi_M T$ for coordination polymer **I**. Insert: plot of thermal variation of χ_M^{-1} for coordination polymer **I**.

presumably because there exists stretching effect of π–π interactions between the coordinated bpy and guest-bpy in **III**. Similarly, corresponding bond angles around Zn(II) ions in **II** and **III** are also different to some extent (selected bond lengths and angles are given in Table 2).[60,61]

Magnetic properties

Variable-temperature magnetic susceptibility of **I** is measured in the temperature range of 2.0–300.0 K. The variation of the inverse magnetic susceptibility χ_M^{-1} and $\chi_M T$ of **I** with temperature is shown in Fig. 7. The thermal evolution of χ_M^{-1} obeys the Curie–Weiss law; namely, $\chi_M = C/(T - \theta)$ in the range of 2–300 K, and Weiss constant θ and Curie constant C_M are −48.416 K and 15.848 cm^3 K mol^{-1}, respectively. The $\chi_M T$ value at 300 K is 13.558 cm^3 K mol^{-1} (10.413 μ_B), and it is much higher than the expected value (8.750 cm^3 K mol^{-1}, 8.365 μ_B) for magnetically isolated high-spin Mn(II) (S_{Mn} = 5/2, g = 2.0). Besides, the $\chi_M T$ value of **I** tends to decrease with declining temperature and it reaches a minimum of 0.588 cm^3 K mol^{-1} at 2.0 K. The negative θ value and the $\chi_M T$ *vs.* T curve of coordination polymer **I** reveal typical antiferromagnetic interactions between the Mn(II) centers. Moreover, the shortest Mn···Mn distance across $(O_2C–C–C–CO_2)_2$ bridge is 5.2297(9) Å, which suggests that the observed antiferromagnetic interaction of **I** should arise from the magnetic super exchange through the $(O_2C–C–C–CO_2)_2$ bridges.[3,22,62]

Thermal analysis

The thermogravimetric (TG) and differential thermogravimetric (DTG) curves of coordination polymers **I**, **II** and **III** are shown in Fig. S4, ESI.† Coordination polymer **I** has weight losses of 3.22%, 22.58%, 14.95% and 5.48% in temperature ranges of 155–220 °C, 260–380 °C, 390–510 °C and 850–925 °C, respectively (relevant calculated weight losses are 2.95%, 23.77%, 14.75% and 6.07%). Coordination polymer **II** has weight losses of 2.63% and 45.44% in temperature ranges of 157–285 °C and 305–529 °C, respectively (relevant calculated weight losses are 2.58% and 44.07%). Besides, coordination polymer **III** loses 2.00%, 60.99%, 10.85% and 4.30% of weight

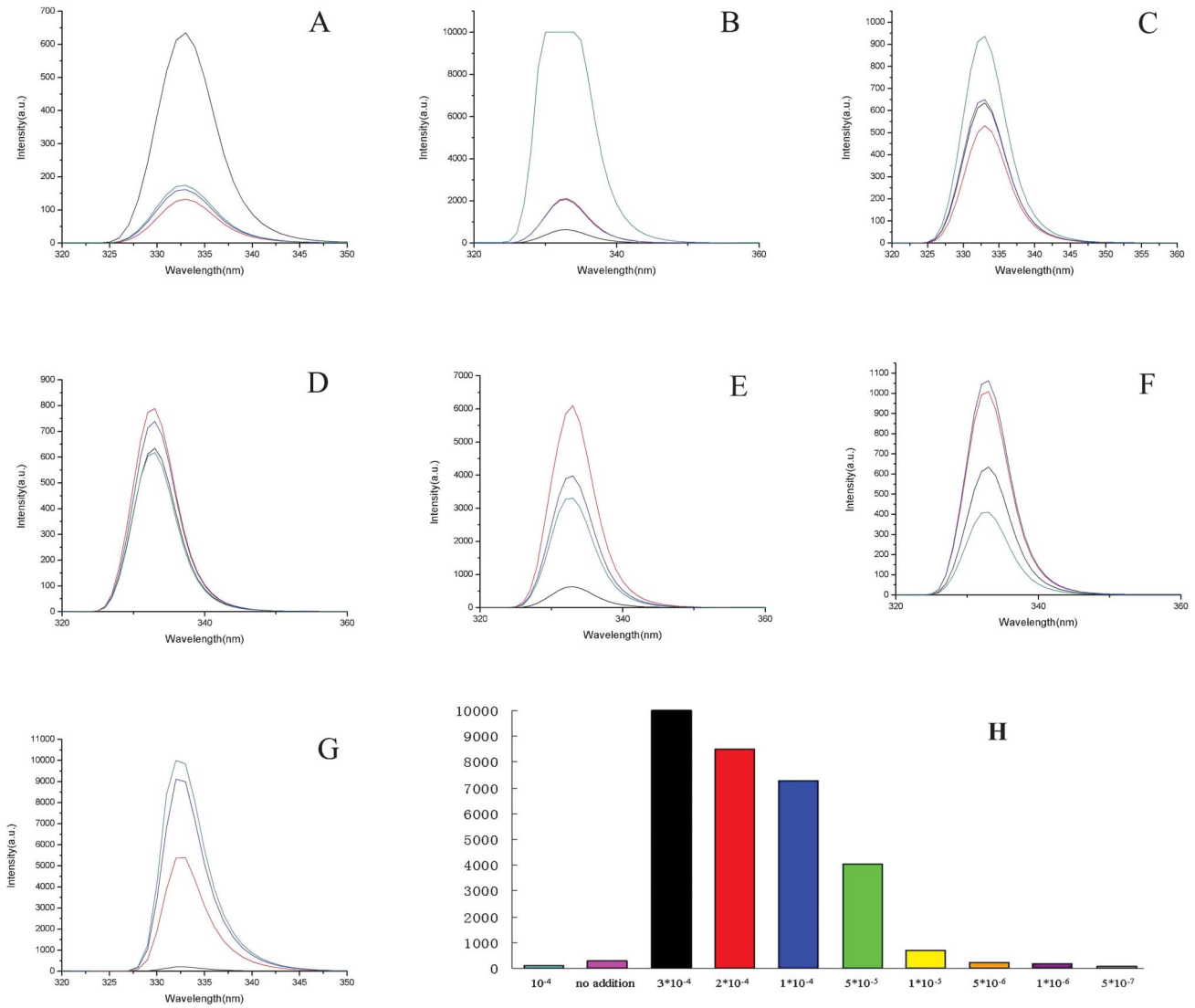

Fig. 8 (A–H): Emission spectra of **II** in water (10^{-4} M) at RT (excited at 287 nm) in the presence of Cu^{2+}, Zn^{2+}, Cd^{2+}, Pb^{2+}, Mn^{2+} and Hg^{+} ions with respect to **II**; A: black, **II** (10^{-4} M); red, H_4bptc; blue, bpy (10^{-4} M); green, $Zn(COO)_2\ H_2O$ (10^{-4} M); B: Cu^{2+}; C: Zn^{2+}; D: Cd^{2+}; E: Pb^{2+}; F: Mn^{2+} and G: Hg^{+} (black, no addition; red, 1 equiv.; blue, 2 equiv.; green, 3 equiv.); (H): luminescent intensity of **II** (10^{-4} M) at 333 nm in water at RT upon addition of different concentrations of Hg^{+} ions (pink: no addition, black: 3×10^{-4}, red: 2×10^{-4}, blue: 1×10^{-4}, green: 5×10^{-5}, yellow: 1×10^{-5}, orange: 5×10^{-6}, purple: 1×10^{-6}, gray: 5×10^{-7} M).

in the temperature ranges of 246–303 °C, 334–508 °C, 510–654 °C and 885–984 °C, respectively (relevant calculated weight losses are 2.44%, 60.55%, 10.59% and 3.84%).

X-ray powder diffraction (XRPD) analysis

To confirm the purity of **III** and investigate whether its 3D porous framework is collapsed upon removal of uncoordinated guest-bpy molecules, we conducted room temperature (RT) XRPD analyses of as-synthesized product **III** and the same sample heated at 340 °C for 12 h (the guest-bpy molecules of as-synthesized **III** are removed after heating). Interestingly, original product **III** and its heated counterpart show the same XRD patterns, which suggests that the crystal lattice and 3D porous framework of as-synthesized product **III** remain intact after its uncoordinated guest-bpy molecules are removed. This is also confirmed by corresponding IR spectra (see Fig. S5, ESI†).

Luminescent properties

To examine the possibility of modifying luminescent properties through cation exchange, we immersed solid sample **II** in water (10^{-4} M) containing various metal cations and measured the luminescent properties of resultant solutions at room temperature. Fig. 8 shows the emission spectra of **II** in water containing Cu^{2+}, Zn^{2+}, Cd^{2+}, Pb^{2+}, Mn^{2+} and Hg^{+} ions (various metal salts are added in the sequences of B: Cu^{2+}; C: Zn^{2+}; D: Cd^{2+}; E: Pb^{2+}; F: Mn^{2+} and G: Hg^{+}). It is seen that, as compared with solid state sample **II**, the counterpart in the aqueous solutions exhibits emission bands with unchanged position but changed intensity (excited at 287 nm). Namely, in the presence of 3×10^{-4} M Cu^{2+} ($Cu(CH_3COO)_2$), the emission

Table 1 Summary of crystallographic data for **I–III**

	I	**II**	**III**
Empirical formula	$C_{65}H_{42}Mn_2N_8O_{11}$	$C_{27}H_{15}Zn_2N_2O_{10}$	$C_{32}H_{20}N_3O_{10}Zn_2$
Formula weight	1220.95	658.15	737.25
Temperature/K	296(2)	296(2)	296(2)
Wavelength/Å	0.71073	0.71073	0.71073
Crystal system	Monoclinic	Monoclinic	Monoclinic
Space group	$C2/c$	$P2_1/n$	$P2_1/n$
a (Å)	24.460(4)	11.0612(16)	11.0632(6)
b (Å)	9.9842(14)	15.0262(17)	15.0159(8)
c (Å)	23.479(3)	16.7833(16)	16.7772(9)
α (°)	90	90	90
β (°)	110.705(3)	95.4910(10)	95.3940(10)
γ (°)	90	90	90
Z	4	4	4
Density (calculated)	1.512 Mg m^{-3}	1.574 Mg m^{-3}	1.765 Mg m^{-3}
F(000)	2504	1324	1492
Crystal size (mm^3)	0.44 × 0.32 × 0.21	0.42 × 0.36 × 0.28	0.41 × 0.40 × 0.26
θ range for data collection (°)	2.07 to 25.00	1.82 to 25.00	1.82 to 25.00
Limiting indices	$-28 \leqslant h \leqslant 28$, $-11 \leqslant k \leqslant 11$, $-17 \leqslant l \leqslant 27$	$-13 \leqslant h \leqslant 12$, $-17 \leqslant k \leqslant 17$, $-19 \leqslant l \leqslant 14$	$-13 \leqslant h \leqslant 8$, $-15 \leqslant k \leqslant 17$, $-19 \leqslant l \leqslant 19$
Reflections collected/unique	13 329/4710 [R_{int} = 0.0375]	13 898/4884 [R_{int} = 0.0249]	13 891/4873 [R_{int} = 0.0196]
Refinement method	Full-matrix least-squares on F^2	Full-matrix least-squares on F^2	Full-matrix least-squares on F^2
Data/restraints/parameters	4710/0/389	4884/0/371	4873/0/424
Goodness-of-fit on F^2	1.073	1.039	1.078
Volume (Å^3)	5363.6(13)	2776.7(6)	2774.8(3)
Final R indices [$I > 2\sigma(I)$]	R_1 = 0.0441, wR_2 = 0.1279	R_1 = 0.0317, wR_2 = 0.0816	R_1 = 0.0312, wR_2 = 0.0862
R indices (all data)	R_1 = 0.0602, wR_2 = 0.1355	R_1 = 0.0397, wR_2 = 0.0846	R_1 = 0.0378, wR_2 = 0.0887
Largest diff. peak and hole (e Å^{-3})	1.627 and −0.238	0.677 and −0.350	0.587 and −0.569

spectrum of **II** at 333 nm is enhanced by nearly 20 times (see spectrum B in Fig. 8). Upon the addition of 1 × 10^{-4}–3 × 10^{-4} M Zn^{2+} ($Zn(CH_3COO)_2$), the emission intensity of **II** is gradually enhanced (see spectrum C in Fig. 8); and the introduction of 1 × 10^{-4}–3 × 10^{-4} M Cd^{2+} ($Cd(CH_3COO)_2$) leads to gradual decrease of the emission intensity of **II** (see spectrum D in Fig. 8). In the presence of 1 × 10^{-4}–3 × 10^{-4} M Pb^{2+} ($Pd(CH_3COO)_2$), the emission intensities of **II** at 333 nm are significantly enhanced by about 10 to 20 times (see spectrum E in Fig. 8). Moreover, the introduction of 1 × 10^{-4} M and 2 × 10^{-4} M Mn^{2+} ($Mn(CH_3COO)_2$) enhances the emission intensity of **II** at 333 nm, but the emission intensity is nearly reduced by about 50% upon adding 3 × 10^{-4} M Mn^{2+} (see spectrum F in Fig. 8). In addition, the emission intensities are enhanced dramatically upon the addition of 1–3 equivalent (abridged as equiv.) Hg^+ ion ($Hg_2(NO_3)_2$); namely, the addition of 1 × 10^{-4} M, 2 × 10^{-4} M, and 3 × 10^{-4} M Hg^+ ion results in an increase of the emission peak intensities of **II** at 333 nm by 20–30 times (see spectrum G in Fig. 8). Reasonably, the emission intensities weaken gradually with the attenuation of added Hg^+ ion; and in particular, when the concentration of Hg^+ ion reaches 5 × 10^{-7} M, the emission spectrum of **II** is nearly quenched (see spectrum H in Fig. 8).

Since the luminescent intensity of Zn(II) relies on the efficiency of energy transfer from the ligand to Zn(II) center,[63,64] we can suppose that the emission of **II** is closely related to the ligand-to-metal-charge-transfer (LMCT).[65] Namely, the enhanced luminescent intensities of **II** in aqueous solution may result from more effective intramolecular energy transfer from the bptc ligands to the central Zn(II); and this energy transfer process is accelerated upon the introduction of certain transition metal ions.[66] In one word, metal ions have significant effect on the luminescent intensities of **II** in aqueous solution, and the luminescent emission of **II** displays selectivity towards a certain concentration of Cu^{2+}, Pb^{2+} and particularly Hg^+. To further elucidate the possible recognition mechanism of **II** towards various metal ions, we have made efforts to obtain single crystal Hg^+ connected with **II** in water but without success so far.

Conclusion

We report here three novel coordination polymers generated from 3,3′,4,4′-benzophenone-tetracarboxylate in the presence of 4,4′-bipyridine auxiliary ligand or 1,10-phenanthroline auxiliary ligand. Structural characterization results of as-synthesized coordination polymers demonstrate that bptc ligand exhibits remarkable versatility to chelate metals in different coordination modes thereby resulting in different interesting topological frameworks. In the meantime, the coordination conformation and deprotonation of bptc ligand can be readily adjusted by properly controlling pH value of the reaction system, which makes it feasible to construct desired reaction-controllable polymeric architectures in a facile manner. Besides, ligands 4,4′-bipyridine and 1,10-phenanthroline as reaction templates and deprotonation reagents play important roles in synthesizing target coordination polymers. Moreover, porous coordination polymers **II** and **III** are similar in terms of coordination chemistry, except that nanosized cavities are empty in **II** but are occupied by uncoordinated

Table 2 Selected bond lengths (Å) and bond angles (°) for **I–III**[a]

Bond lengths			
I			
Mn(1)–O(2)	2.791(2)	Mn(1)–N(4)	2.308(2)
Mn(1)–O(3)	2.157(2)	Mn(1)–N(2)	2.332(2)
Mn(1)–O(4)	2.105(2)	Mn(1)–N(3)	2.467(3)
Mn(1)–N(1)	2.293(2)		
II			
Zn(1)–O(1)	1.9563(19)	Zn(2)–O(8)	2.048(2)
Zn(1)–O(6)	1.9587(19)	Zn(2)–N(2)#3	2.053(2)
Zn(1)–O(4)#2	1.9816(18)	Zn(2)–O(2)	2.089(2)
Zn(1)–N(1)	2.040(2)	Zn(2)–O(11)	2.184(2)
Zn(2)–O(3)	1.989(2)	Zn(2)–O(9)	2.487(3)
III			
Zn(1)–O(1)#1	1.9570(19)	Zn(2)–O(7)	2.051(2)
Zn(1)–O(6)	1.9581(19)	Zn(2)–O(3)#4	2.080(2)
Zn(1)–O(9)#2	1.9786(19)	Zn(2)–O(1W)	2.143(2)
Zn(1)–N(2)#3	2.044(2)	Zn(2)–O(4)#4	2.315(3)
Zn(2)–O(8)	1.996(2)	Zn(2)–C(8)#4	2.498(3)
Zn(2)–N(1)	2.050(2)		
Bond angles			
I			
O(4)–Mn(1)–O(3)	100.81(8)	N(1)–Mn(1)–N(2)	71.63(8)
O(4)–Mn(1)–N(1)	164.98(8)	N(4)–Mn(1)–N(2)	144.33(8)
O(3)–Mn(1)–N(1)	82.32(8)	O(4)–Mn(1)–N(3)	91.79(8)
O(4)–Mn(1)–N(4)	106.38(8)	O(3)–Mn(1)–N(3)	153.73(8)
O(3)–Mn(1)–N(4)	84.98(8)	N(1)–Mn(1)–N(3)	91.46(8)
N(1)–Mn(1)–N(4)	88.48(8)	N(4)–Mn(1)–N(3)	69.30(8)
O(4)–Mn(1)–N(2)	94.37(8)	N(2)–Mn(1)–N(3)	81.61(8)
O(3)–Mn(1)–N(2)	119.78(8)		
II			
O(1)–Zn(1)–O(6)	118.03(8)	N(2)#3–Zn(2)–O(2)	91.02(9)
O(1)–Zn(1)–O(4)#2	113.95(8)	O(3)–Zn(2)–O(11)	91.76(9)
O(6)–Zn(1)–O(4)#2	107.32(8)	O(8)–Zn(2)–O(11)	89.79(9)
O(1)–Zn(1)–N(1)	108.52(9)	N(2)#3–Zn(2)–O(11)	94.84(9)
O(6)–Zn(1)–N(1)	106.31(9)	O(2)–Zn(2)–O(11)	174.13(8)
O(4)#2–Zn(1)–N(1)	101.12(8)	O(3)–Zn(2)–O(9)	104.82(9)
O(3)–Zn(2)–O(8)	161.16(10)	O(8)–Zn(2)–O(9)	57.09(10)
O(3)–Zn(2)–N(2)#3	97.70(9)	N(2)#3–Zn(2)–O(9)	156.80(9)
O(8)–Zn(2)–N(2)#3	100.88(10)	O(2)–Zn(2)–O(9)	95.58(9)
O(3)–Zn(2)–O(2)	87.01(9)	O(11)–Zn(2)–O(9)	79.18(9)
O(8)–Zn(2)–O(2)	89.53(10)		
III			
O(1)#1–Zn(1)–O(6)	117.77(8)	O(7)–Zn(2)–O(1W)	174.91(8)
O(1)#1–Zn(1)–O(9)#2	107.59(9)	O(3)#4–Zn(2)–O(1W)	89.11(8)
O(6)–Zn(1)–O(9)#2	113.81(8)	O(8)–Zn(2)–O(4)#4	108.03(9)
O(1)#1–Zn(1)–N(2)#3	105.95(9)	N(1)–Zn(2)–O(4)#4	157.11(9)
O(6)–Zn(1)–N(2)#3	108.57(9)	O(7)–Zn(2)–O(4)#4	93.92(9)
O(9)#2–Zn(1)–N(2)#3	101.66(8)	O(3)#4–Zn(2)–O(4)#4	59.69(9)
O(8)–Zn(2)–N(1)	94.53(9)	O(1W)–Zn(2)–O(4)#4	81.15(9)
O(8)–Zn(2)–O(7)	88.06(9)	O(8)–Zn(2)–C(8)#4	137.41(11)
N(1)–Zn(2)–O(7)	90.58(9)	N(1)–Zn(2)–C(8)#4	128.01(10)
O(8)–Zn(2)–O(3)#4	167.27(9)	O(7)–Zn(2)–C(8)#4	92.96(10)
N(1)–Zn(2)–O(3)#4	97.98(9)	O(3)#4–Zn(2)–C(8)#4	30.33(10)
O(7)–Zn(2)–O(3)#4	89.47(9)	O(1W)–Zn(2)–C(8)#4	83.36(9)
O(8)–Zn(2)–O(1W)	92.27(9)	O(4)#4–Zn(2)–C(8)#4	29.39(10)
N(1)–Zn(2)–O(1W)	94.46(9)		

[a] Symmetry transformations used to generate equivalent atoms: for **II** #1 $-x + 3/2$, $y - 1/2$, $-z + 1/2$ #2 $-x + 2$, $-y + 1$, $-z$ #3 $-x + 3/2$, $y + 1/2$, $-z + 1/2$ For **III** #1 $-x + 1/2$, $y - 1/2$, $-z - 1/2$ #2 $-x + 1$, $-y$, $-z$ #3 $-x + 1/2$, $y + 1/2$, $-z + 1/2$ #4 $-x + 1$, $-y + 1$, $-z$.

4,4′-bpy guest molecules in **III**. Particularly, product **I** presents antiferromagnetic coupling through the $(O_2C–C–C–CO_2)_2$ bridges, while product **II** displays selective recognition towards Hg^+ ions in terms of the luminescent properties and may be a good candidate as luminescent material.

Table 3 Hydrogen bond geometry (Å/°) in **I**[a]

D–H···A	*d*(D–H)	*d*(H···A)	*d*(D···A)	∠(D–H···A)
O(1W)–H(1WA)···O(5)	0.85	2.18	3.020(3)	167.9
O(1W)–H(1WB)···O(5)#3	0.85	2.29	3.111(3)	161.9
O(1W)–H(1WB)···O(4)#3	0.85	2.39	3.102(3)	141.0

[a] Symmetry transformations used to generate equivalent atoms: #3 $-x + 1/2$, $-y + 3/2$, $-z + 1$.

Experimental section

Materials and physical measurements

All chemicals were commercially purchased and used without further purification. Elemental analyses (C, H, and N) were performed with a Perkin-Elmer 240 CHN Elemental Analyzer. IR spectra in the range of 400–4000 cm^{-1} were recorded with an AVATAR 360 FT-IR spectrometer (KBr pellets were used). The crystal structure was determined with a Bruker Smart CCD X-ray single-crystal diffractometer. TG analysis was conducted with a Perkin-Elmer TGA7 instrument in flowing N_2 at a heating rate of 10 °C min^{-1}. Excitation and emission spectra were obtained with an F-7000 FL spectrofluorometer at room temperature. Magnetic susceptibility measurements were conducted with a Quantum Design MPMS-5 magnetometer in the temperature range of 2.0–300.0 K. A DX-2700 X-ray powder diffractometer was performed at a scan rate of 6° min^{-1} in a 2θ range of 5°–45° to record the XRPD patterns of as-synthesized product **III** and the same sample heated at 340 °C for 12 h.

Synthesis of I, II, and III

$\{[Mn_2(bptc)_2(phen)_4]\cdot 2H_2O\}_\infty$ (I). A mixture of manganese acetate (0.25 mmol), 3,3′,4,4′-benzophenone-tetracarboxylate (0.25 mmol), 1,10-phenanthroline (0.25 mmol) and water (10 mL) in an 25 mL Teflon-lined stainless autoclave was adjusted to pH 5.0 with 1 mol L^{-1} NaOH solution. The mixture was then heated at 170 °C for 4 days to afford yellowish block-shaped crystals in 59.4% yield after slowly cooling to room temperature. Elemental analysis calculated (mass fraction, the same hereafter) for $C_{65}H_{42}Mn_2N_8O_{11}$ (1220.95): C 63.94%, H 3.47%, N 9.18%. Found: C 64.02%, H 3.59%, N 9.07%. Selected IR (cm^{-1}): 3425(s), 1630(s), 1575(s), 1515(m), 1483(w), 1424(s), 1402(s), 1301(w), 1279(w), 1245(w), 1229(w), 1142(w), 1102(w), 1084(w), 1048(w), 1007(w), 912(w), 850(m), 764(w), 730(s), 666(w), 638(w), 476(w), 420(w).

$[Zn_2(bptc)_4\cdot(bpy)_2\cdot H_2O]_\infty$ (II). A mixture of zinc acetate (0.25 mmol), 3,3′,4,4′-benzophenone-tetracarboxylate (0.25 mmol) and 4,4′-bipyridine (0.25 mmol) in 10 mL of water was adjusted to pH 5.5 with 1 mol L^{-1} NaOH solution. The mixture was then transferred to and sealed in a 25 mL Teflon-lined stainless autoclave, followed by heating at 160 °C for 4 days to afford yellowish block-shaped crystals in 69.2% yield after slowly cooling to room temperature. Elemental analysis calculated for $C_{27}H_{15}Zn_2N_2O_{10}$ (658.15): C 49.27%, H 2.30%, N 4.26%. Found: C 49.78%, H 2.21%, N 4.52%. Selected IR (cm^{-1}): 3364(m), 3110(m), 3060(m), 1672(m), 1613(s), 1568(s), 1493(m), 1414(s), 1363(s), 1300(m), 1244(m), 1220(m), 1178(w),

1135(w), 1083(m), 1071(m), 1047(w), 1015(w), 997(w), 913(s), 853(s), 805(w), 771(m), 755(m), 725(w), 709(m), 673(m), 643(m), 613(w), 587(w), 522(m), 462(w), 409(w).

{[Zn_2(bptc)$_4$·(bpy)$_2$·H_2O] ⊃ bpy}$_\infty$ (III). A mixture of zinc acetate (0.125 mmol), cadmium acetate (0.125 mmol), 3,3′,4,4′-benzophenone-tetracarboxylate (0.25 mmol) and 4,4′-bipyridine (0.25 mmol) in 10 mL of water was adjusted to pH 5.5 with 1 mol L^{-1} NaOH solution. The mixture was then transferred to and sealed in a 25 mL Teflon-lined stainless autoclave, followed by heating at 160 °C for 4 days to afford yellowish block-shaped crystals in 74.7% yield after slowly cooling to room temperature. Elemental analysis calculated for $C_{32}H_{20}Zn_2N_3O_{10}$ (737.25): C 52.99%, H 2.41%, N 5.11%. Found: C 52.13%, H 2.73%, N 5.70%. Selected IR (cm^{-1}): 3373(m), 3110(m), 3060(m), 1654(m), 1610(s), 1553(s), 1473(m), 1412(s), 1373(s), 1311(m), 1239(m), 1221(m), 1177(w), 1130(w), 1086(m), 1072(m), 1037(w), 1013(w), 991(w), 908(s), 849(s), 802(w), 782(m), 743(m), 737(w), 701(m), 632(m), 614(m), 603(w), 593(w), 517(m), 443(w), 404(w).

Crystallographic data collection and refinement

Single-crystal diffraction data of suitable single crystals of coordination polymers **I**, **II** and **III** were measured with a Bruker Smart CCD X-ray single-crystal diffractometer (graphite monochromated Mo Kα radiation, λ = 0.71073 Å) at 296(2) K. All independent reflections were collected in a 2θ range of 2.07–25.00° for **I**, 1.82–25.00° for **II** and 1.82–25.00° for **III** (determined in subsequent refinement). Multi-scan empirical absorption corrections were applied to process the single crystal diffraction data with the SADABS.[61] The crystal structure was solved by direct methods and Fourier synthesis. Positional and thermal parameters were refined by the full-matrix least-squares method on F^2 with the SHELXTL[67] software package. The final least-square cycle of refinement gives R_1 = 0.0441 and wR_2 = 0.1279 for **I**, R_1 = 0.0317 and wR_2 = 0.0816 for **II**, and R_1 = 0.0312 and wR_2 = 0.0862 for **III**. The weighting schemes for **I**, **II**, and **III** are expressed as w = 1/[$\sigma^2(F_o^2)$ + (0.0752P)^2 + 2.54P], w = 1/[$\sigma^2(F_o^2)$ + (0.10000P)^2 + 0.00P], and w = 1/[$\sigma^2(F_o^2)$ + (0.0472P)^2 + 2.30P], respectively; where $P = (F_o^2 + 2F_c^2)/3$. A summary of the key crystallographic information is given in Table 1. Selected bond lengths and bond angles for **I**, **II**, and **III** are listed in Table 2.

Acknowledgements

This research was financially supported by the Natural Science Foundation of Henan Province of China (Nos. 13A150056, 2012B150005, 122102210174 and 2012B150004).

Notes and references

1 M. Fang, L. Chang, X. Liu, B. Zhao, Y. Zuo and Z. Chen, *Cryst. Growth Des.*, 2009, **9**, 4006–4016.
2 S. K. Ghosh, J. Ribas and P. K. Bharadwaj, *CrystEngComm*, 2004, **6**, 250–256.
3 D. R. Xiao, E. B. Wang, H. Y. An, Y. G. Li, Z. M. Su and C. Y. Sun, *Chem.–Eur. J.*, 2006, **12**, 6528–6541.
4 X.-L. Wang, C. Qin and E.-B. Wang, *Cryst. Growth Des.*, 2006, **6**, 439–443.
5 E. J. Gao, M. Su, M. Zhang, Y. Huang, L. Wang, M. C. Zhu, L. Liu, Y. X. Zhang, M. J. Guo and F. Guan, *Z. Anorg. Allg. Chem.*, 2010, **636**, 1565–1569.
6 C.-C. Wang, P. Wang and G.-S. Guo, *Transition Met. Chem.*, 2010, **35**, 721–729.
7 L.-X. Sun, Y. Qi, Y.-M. Wang, Y.-X. Che and J.-M. Zheng, *CrystEngComm*, 2010, **12**, 1540–1547.
8 J. Zhang, Z.-J. Li, Y. Kang, J.-K. Cheng and Y.-G. Yao, *Inorg. Chem.*, 2004, **43**, 8085–8091.
9 L. Carlucci, G. Ciani and D. M. Proserpio, *Coord. Chem. Rev.*, 2003, **246**, 247–289.
10 A. Y. Robin and K. M. Fromm, *Coord. Chem. Rev.*, 2006, **250**, 2127–2157.
11 S. Masaoka, S. Furukawa, H. C. Chang, T. Mizutani and S. Kitagawa, *Angew. Chem., Int. Ed.*, 2001, **40**, 3817–3819.
12 W. L. Leong and J. J. Vittal, *Chem. Rev.*, 2011, **111**, 688–764.
13 R. J. Hill, D.-L. Long, P. Hubberstey, M. Schröder and N. R. Champness, *J. Solid State Chem.*, 2005, **178**, 2414–2419.
14 T. M. Reineke, M. Eddaoudi, M. Fehr, D. Kelley and O. Yaghi, *J. Am. Chem. Soc.*, 1999, **121**, 1651–1657.
15 K. Biradha, Y. Hongo and M. Fujita, *Angew. Chem., Int. Ed.*, 2002, **41**, 3395–3398.
16 J. Kim, B. Chen, T. M. Reineke, H. Li, M. Eddaoudi, D. B. Moler, M. O'Keeffe and O. M. Yaghi, *J. Am. Chem. Soc.*, 2001, **123**, 8239–8247.
17 S. D. Walker, T. E. Barder, J. R. Martinelli and S. L. Buchwald, *Angew. Chem., Int. Ed.*, 2004, **43**, 1871–1876.
18 C.-Y. Su, A. M. Goforth, M. D. Smith, P. Pellechia and H.-C. zur Loye, *J. Am. Chem. Soc.*, 2004, **126**, 3576–3586.
19 K. Campbell, C. J. Kuehl, M. J. Ferguson, P. J. Stang and R. R. Tykwinski, *J. Am. Chem. Soc.*, 2002, **124**, 7266–7267.
20 S.-L. Li, Y.-Q. Lan, J.-F. Ma, J. Yang, G.-H. Wei, L.-P. Zhang and Z.-M. Su, *Cryst. Growth Des.*, 2008, **8**, 675–684.
21 S.-L. Li, Y.-Q. Lan, J.-C. Ma, J.-F. Ma and Z.-M. Su, *Cryst. Growth Des.*, 2010, **10**, 1161–1170.
22 H. Wang, Y.-Y. Wang, G.-P. Yang, C.-J. Wang, G.-L. Wen, Q.-Z. Shi and S. R. Batten, *CrystEngComm*, 2008, **10**, 1583–1594.
23 Y.-N. Zhang, H. Wang, J.-Q. Liu, Y.-Y. Wang, A.-Y. Fu and Q.-Z. Shi, *Inorg. Chem. Commun.*, 2009, **12**, 611–614.
24 O. M. Yaghi, M. O'Keeffe, N. W. Ockwig, H. K. Chae, M. Eddaoudi and J. Kim, *Nature*, 2003, **423**, 705–714.
25 S. Hasegawa, S. Horike, R. Matsuda, S. Furukawa, K. Mochizuki, Y. Kinoshita and S. Kitagawa, *J. Am. Chem. Soc.*, 2007, **129**, 2607.
26 B. Chen, X. Zhao, A. Putkham, K. Hong, E. B. Lobkovsky, E. J. Hurtado, A. J. Fletcher and K. M. Thomas, *J. Am. Chem. Soc.*, 2008, **130**, 6411–6423.
27 M. Eddaoudi, D. B. Moler, H. Li, B. Chen, T. M. Reineke, M. O'keeffe and O. M. Yaghi, *Acc. Chem. Res.*, 2001, **34**, 319–330.
28 P. Schwerdtfeger, *Angew. Chem., Int. Ed.*, 2003, **42**, 1892–1895.
29 A. P. Côté, A. I. Benin, N. W. Ockwig, M. O'Keeffe, A. J. Matzger and O. M. Yaghi, *Science*, 2005, **310**, 1166–1170.

30 H. K. Chae, D. Y. Siberio-Pérez, J. Kim, Y. Go, M. Eddaoudi, A. J. Matzger, M. O'Keeffe and O. M. Yaghi, *Nature*, 2004, **427**, 523–527.
31 N. L. Rosi, M. Eddaoudi, J. Kim, M. O'Keeffe and O. M. Yaghi, *Angew. Chem.*, 2002, **114**, 294–297.
32 N. L. Rosi, J. Kim, M. Eddaoudi, B. Chen, M. O'Keeffe and O. M. Yaghi, *J. Am. Chem. Soc.*, 2005, **127**, 1504–1518.
33 D. J. Tranchemontagne, J. L. Mendoza-Cortés, M. O'Keeffe and O. M. Yaghi, *Chem. Soc. Rev.*, 2009, **38**, 1257–1283.
34 C. Mellot Draznieks, J. M. Newsam, A. M. Gorman, C. M. Freeman and G. Férey, *Angew. Chem., Int. Ed.*, 2000, **39**, 2270–2275.
35 M. P. Suh, Y. E. Cheon and E. Y. Lee, *Coord. Chem. Rev.*, 2008, **252**, 1007–1026.
36 M. Eddaoudi, J. Kim, N. Rosi, D. Vodak, J. Wachter, M. O'Keeffe and O. M. Yaghi, *Science*, 2002, **295**, 469–472.
37 X. Zhao, D. Liang, S. Liu, C. Sun, R. Cao, C. Gao, Y. Ren and Z. Su, *Inorg. Chem.*, 2008, **47**, 7133–7138.
38 A. J. Blake, N. R. Champness, P. Hubberstey, W.-S. Li, M. A. Withersby and M. Schröder, *Coord. Chem. Rev.*, 1999, **183**, 117–138.
39 R. S. Rarig Jr, R. Lam, P. Y. Zavalij, J. K. Ngala, R. L. LaDuca Jr, J. E. Greedan and J. Zubieta, *Inorg. Chem.*, 2002, **41**, 2124–2133.
40 B. Chen, M. Eddaoudi, S. Hyde, M. O'keeffe and O. Yaghi, *Science*, 2001, **291**, 1021–1023.
41 G. Férey, C. Mellot-Draznieks, C. Serre, F. Millange, J. Dutour, S. Surblé and I. Margiolaki, *Science*, 2005, **309**, 2040–2042.
42 M. D. Stephenson and M. J. Hardie, *Cryst. Growth Des.*, 2006, **6**, 423–432.
43 H. W. Roesky and M. Andruh, *Coord. Chem. Rev.*, 2003, **236**, 91–119.
44 M. J. Plater, S. J. Foreman, R. Mark, R. A. Howie, J. Skakle and A. M. Slawin, *Inorg. Chim. Acta*, 2001, **315**, 126–132.
45 J. A. Cowan, J. A. Howard, G. J. McIntyre, S.-F. Lo and I. D. Williams, *Acta Crystallogr., Sect. B: Struct. Sci.*, 2003, **59**, 794–801.
46 A. Lough, P. Wheatley, G. Ferguson and C. Glidewell, *Acta Crystallogr., Sect. B: Struct. Sci.*, 2000, **56**, 261–272.
47 X.-Y. Yu, X.-B. Cui, X. Zhang, L. Jin, Y.-N. Luo, J.-J. Yang, H. Zhang and X. Zhao, *Inorg. Chem. Commun.*, 2011, **14**, 848–851.
48 M. Tabatabaee, M. A. Sharif, F. Vakili and S. Saheli, *J. Rare Earths*, 2009, **27**, 356–361.
49 S.-M. Fang, M. Hu, Q. Zhang, M. Du and C.-S. Liu, *Dalton Trans.*, 2011, **40**, 4527–4541.
50 G. J. McManus, J. J. Perry IV, M. Perry, B. D. Wagner and M. J. Zaworotko, *J. Am. Chem. Soc.*, 2007, **129**, 9094–9101.
51 Z. Shi, G.-H. Li, L. Wang, L. Gao, X.-B. Chen, J. Hua and S.-h. Feng, *Cryst. Growth Des.*, 2004, **4**, 25–27.
52 L.-G. Qiu, A.-J. Xie and L.-D. Zhang, *Adv. Mater.*, 2005, **17**, 689–692.
53 Q.-R. Fang, X. Shi, G. Wu, G. Tian, G.-S. Zhu, R.-W. Wang and S.-L. Qiu, *J. Solid State Chem.*, 2003, **176**, 1–4.
54 M. Osawa, J. M. Chalmers and P. R. Griffiths, *Handbook of Vibrational Spectroscopy*, Wiley, Chichester, 2002, 1, 785.
55 Y.-Y. Liu, H.-J. Li, Y. X.-F. Lv, H.-W. Hou and Y.-T. Fan, *Cryst. Growth Des.*, 2012, **12**, 3505–3513.
56 G.-X. Liu, X.-C. Cha, X.-L. Li, C.-Y. Zhang, Y. Wang, S. Nishihara and X.-M. Ren, *Inorg. Chem. Commun.*, 2011, **14**, 867–872.
57 Q.-B. Bo, Z.-X. Sun, G.-L. Song, F. Li and G.-X. Sun, *J. Inorg. Organomet. Polym. Mater.*, 2007, **17**, 615–622.
58 S.-Q. Zang, R. Liang, Y.-J. Fan, H.-W. Hou and T. C. Mak, *Dalton Trans.*, 2010, **39**, 8022–8032.
59 C.-F. Zhuang, J. Zhang, Q. Wang, Z.-H. Chu, D. Fenske and C.-Y. Su, *Chem.–Eur. J.*, 2009, **15**, 7578–7585.
60 R. Kitaura, S. Kitagawa, Y. Kubota, T. C. Kobayashi, K. Kindo, Y. Mita, A. Matsuo, M. Kobayashi, H.-C. Chang and T. C. Ozawa, *Science*, 2002, **298**, 2358–2361.
61 R. Matsuda, R. Kitaura, S. Kitagawa, Y. Kubota, T. C. Kobayashi, S. Horike and M. Takata, *J. Am. Chem. Soc.*, 2004, **126**, 14063–14070.
62 F. Zhang, Z. Li, T. Ge, H. Yao, G. Li, H. Lu and Y. Zhu, *Inorg. Chem.*, 2010, **49**, 3776–3788.
63 L.-R. Yang, S. Song, C.-Y. Shao, W. Zhang, H.-M. Zhang, Z.-W. Bu and T.-G. Ren, *Synth. Met.*, 2011, **161**, 925–930.
64 H. Yin and S.-X. Liu, *J. Mol. Struct.*, 2009, **918**, 165–173.
65 H.-L. Gao, L. Yi, B. Zhao, X.-Q. Zhao, P. Cheng, D.-Z. Liao and S.-P. Yan, *Inorg. Chem.*, 2006, **45**, 5980–5988.
66 B. Zhao, X.-Y. Chen, P. Cheng, D.-Z. Liao, S.-P. Yan and Z.-H. Jiang, *J. Am. Chem. Soc.*, 2004, **126**, 15394–15395.
67 G. M. Sheldrick, *SHELXTL, version 5, Reference manual*, Siemens Analytical X-ray Systems, USA, 1996.

